Wide-field-of-view GaAs/Al_xO_y one-dimensional photonic crystal filter

Chyong-Hua Chen, Kevin Tetz, Wataru Nakagawa, and Yeshaiahu Fainman

The design, fabrication, and characterization of a one-dimensional photonic crystal optical filter that has a relatively narrow, flat-topped passband within a wide stop band and small angular sensitivity is presented. The filter is based on a one-dimensional photonic crystal structure that has multiple defects, facilitating simultaneous minimization of the angular sensitivity and optimization of the passband's characteristics. We use epitaxially grown and selectively oxidized GaAs/Al_xO_y multilayers to achieve a high-index-contrast material system and incorporate the experimentally determined optical and material properties into the design of the device. A flat-topped bandpass filter with a bandwidth of 65 nm and a wide field of view of 50° is experimentally characterized and compared with the design predictions.

OCIS codes: 310.6860, 350.2460, 310.1860, 230.4170.

1. Introduction

An optical filter that has a wide range of acceptance angles (wide angular bandwidth) and simultaneously a narrow spectral (i.e., wavelength) passband would be extremely useful in a free-space optical communication system among mobile nodes for which the relative bearing of the transmitter–receiver pair is unknown. Such a filter will reject the out-of-passband ambient light coming from the environment (e.g., Sun, Moon, and other sources). The transmission bandwidth of such a filter needs to be wide enough to transmit the information-carrying beam consisting of the optical carrier and the sidebands. Such functionality can be achieved by introduction of a narrow, flat-topped transmission band into a broad stop band. The design of such a spectral filter operating with a wide angular bandwidth requires special attention, as these two characteristics (i.e., angle and wavelength) are not independent.

The most common technique for implementation of spectral filters is to use a planar multilayer structure. The design approaches for and performance characteristics of such structures are well known,[1,2] as is the dependence of the resonant wavelength of the filter on the incidence angle. Although some techniques to eliminate this dependence in one-dimensional (1-D) structures—such as use of birefringent materials[3]—do exist, they require specialized materials. Other techniques, such as use of wide-angle light collectors,[4–6] reduce the angular sensitivity but at the cost of added fabrication or mechanical complexity of the device. Finally, some methods to optimize the design of a planar multilayer structure directly for reduced angular sensitivity in optical communications applications have been studied,[1] but to the best of our knowledge they have not been thoroughly investigated or experimentally characterized.

In addition, wide-field-of-view filters based on resonant cavities in two-dimensional photonic crystals (PCs) have also been studied.[7] However, with current technology such two-dimensional structures are difficult to achieve because of the complexity of their fabrication, which requires high-aspect-ratio etching steps with small feature sizes for achieving the desired performance at the telecommunication wavelengths of interest, i.e., ~1500 nm. Fortunately, the key characteristics and techniques of multidimensional PCs can also be applied to 1-D multilayer structures. For example, a significant amount of effort has been devoted to the design, analysis, and fabrication of dielectric mirrors made from high-refractive-index contrast material systems—called

C.-H. Chen (chyong@ece.ucsd.edu), K. Tetz, and Y. Fainman are with the Department of Electrical and Computer Engineering, University of California, San Diego, 9500 Gilman Drive, La Jolla, California 92093-0407. W. Nakagawa is with The Institute of Microtechnology, University of Neuchâtel, Rue A.-L. Breguet 2, 2000 Neuchâtel, Switzerland.

Received 12 July 2004; revised manuscript received 3 November 2004; accepted 8 November 2004.

0003-6935/05/081503-09$15.00/0

omnidirectional reflectors—for which the reflection bandwidth is optimized for the broadest spectral and angular bandwidth.[8,9] Although a 1-D PC filter is fundamentally also a multilayer interference filter, the combination of the extensive tools and techniques of planar thin-film filter design with key design ideas from the field of PC devices facilitates the optimization of the multilayer filter for wide-field-of-view, narrow-passband characteristics.

In this paper we present the design, fabrication, and characterization of a wide-field-of-view narrowband wavelength filter that is constructed similarly to a 1-D PC structure with multiple defects (i.e., resonant cavities). The primary defect in the resonant cavity is obtained with the highest possible index of refraction to minimize the variation of the cavity phase with changes in the incidence angle. As the angular dependence of the incidence angle cannot be completely eliminated in an isotropic 1-D structure, the ideal filter would be a perfectly square bandpass filter with a bandwidth that can be specified to match the chosen application. To approximate this type of performance, asymmetric secondary resonant PC cavities, instead of standard multilayer mirrors, surround the primary cavity, resulting in a resonant 1-D PC multilayer structure that has three defects (see Fig. 1). This approach permits control of the spectral reflectivity and phase of each mirror, facilitating control of the transmission spectrum of the device as a whole. Precise engineering of the filter characteristics with respect to wavelength as well as incidence angle is particularly important in applications in which wide acceptance angles (e.g., $\pm 45°$) are required. To demonstrate this novel design approach we fabricated and characterized a filter with a broad stop band designed to transmit a narrowband signal at 1550 nm over a wide range of incidence angles from normal incidence to $\pm 50°$. The fabricated filter consists of 16 alternating layers of GaAs and AlAs grown by molecular beam epitaxy (MBE) and oxidized to produce high refractive-index contrast. The specific optical and geometrical properties of the fabricated structure (indices of refraction, shrinkage in oxidation) were incorporated into the design process, permitting optimization of the design and resulting in excellent agreement between the measured and predicted characteristics of the fabricated device.

In Section 2 we describe the design procedure for achieving a flat-topped, square bandpass filter optimized to minimize the shift in wavelength versus the angle of incidence of the input radiation. In Section 3 we describe the fabrication procedure, which is based on MBE-grown GaAs/AlAs multilayers followed by lateral wet oxidation of AlAs to achieve high refractive-index contrast. In Section 4 we present the results of optical characterization of the filters and compare their measured optical characteristics with the design. Section 5 provides a discussion and conclusions.

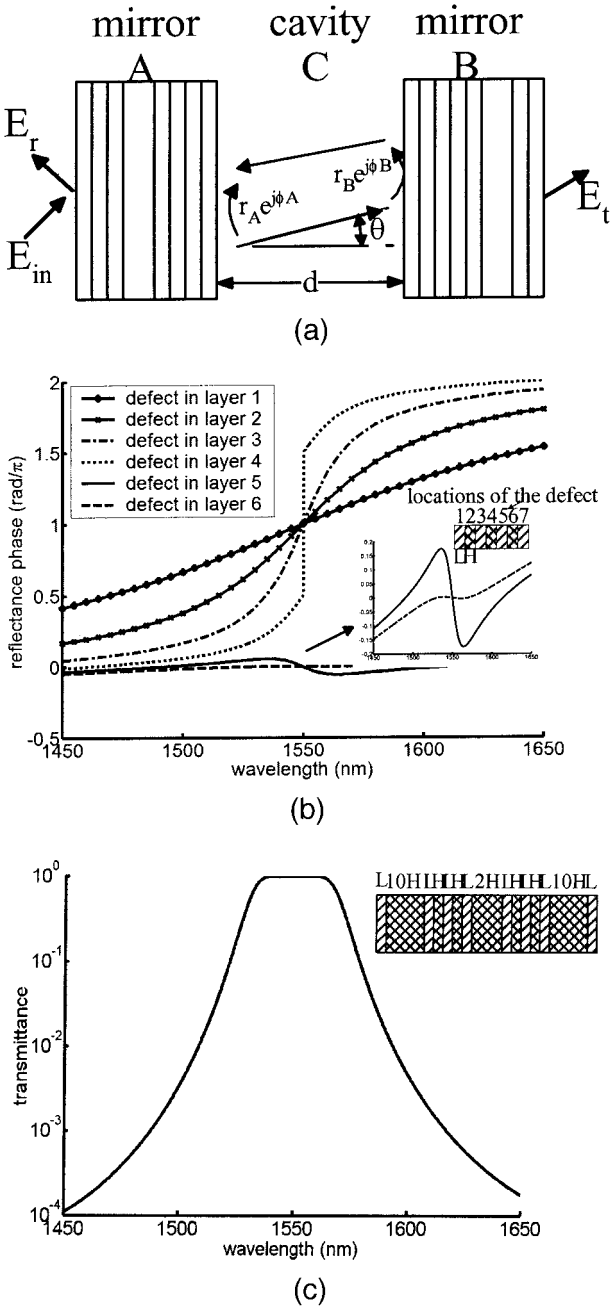

Fig. 1. (a) Schematic diagram of the structure of a bandpass filter consisting of resonant cavity C formed by a pair of mirrors A and B, each with complex reflection–transmission coefficients. (b) Reflectance phase versus wavelength for an AD mirror obtained by use of a seven-layer stack (H|LHLHLHL|H) with $n_H = 3.374$ and $n_L = 1.50$. The optical thickness of L and H is $\lambda_0/4$ at λ_0 1550 nm, and in a defect is introduced into one layer that has the thickness of a full wave, λ_0. Top inset, structure of the seven-layer stack; bottom inset, enlarged curves for the reflectance phases of the AD mirrors with the defect in the fifth or sixth layer. (c) Transmittance of a flat-topped bandpass filter with the structure H|L10HLHLHL2HLHLHL10HL|H.

2. Design of a Filter with a Wide Field of View and a Narrow Spectral Transmission Bandwidth

Our goal is to design a filter that transmits narrowbandwidth laser radiation incident from a wide an-

gular bandwidth range and simultaneously rejects ambient light coming from the environment. Conceptually, a 1-D PC structure made from high-contrast refractive-index materials produces a filter with wide reflectance bandwidth to reject ambient light. By introducing a single defect into the 1-D PC structure we can introduce a narrow transmittance band at the desired optical frequency. Such a design can be seen as a simple Fabry–Perot cavity, transmitting radiation centered at the resonant frequency. The bandwidth of the transmission depends on the reflectivity of the mirrors obtained in our case by the 1-D PC structure. The reflectivity usually needs to be high for good rejection of the out-of-band radiation to be achieved, thereby producing a narrow resonant transmission band in the stop band of such a PC-based filter. Unfortunately, when the angle of incidence in such a 1-D filter changes, the resonant transmission band will shift in wavelength, causing rejection of the desired signal. To overcome this limitation we developed a novel design optimization procedure for wide-field-of-view filters based on introducing multiple resonant cavities into the 1-D PC structure to simultaneously minimize the angular sensitivity of the filter and optimize the passband's shape and width for the specific application.

Consider a bandpass filter structure consisting of two composite mirrors, A and B, creating a cavity C with refractive index n and geometrical thickness d, as shown schematically in Fig. 1(a). Mirrors A and B can be described by their transmittance T_A and T_B and their reflectance R_A and R_B with reflectance phases ϕ_A and ϕ_B, respectively. The transmittance of such a resonant filter consisting of a cavity C with mirrors A and B is given by[2]

$$T = \frac{T_A T_B}{1 + R_A R_B + 2\sqrt{R_A R_B}\cos\Phi}, \quad (1)$$

where Φ is the total phase shift per round trip in the cavity between mirrors A and B, given by

$$\Phi(\omega, \theta) = 2(\omega/c)nd\cos\theta - \phi_A(\omega, \theta) - \phi_B(\omega, \theta), \quad (2)$$

and θ is the orientation of the incident wave vector [Fig. 1(a)].

There are two main components that need to be considered in constructing a filter with a flat-topped transmission passband operating with wide angular bandwidth signals: the flat-topped passband and the wide angular transmittance bandwidth as discussed below. In the following discussion we show results for the TE-polarization state and note that the same approach is applicable to TM polarization.

A. Flat-Topped Passband

A flat-topped transmission band can be obtained under the conditions that $\Phi = (2m + 1)\pi$ and $d\Phi/d\omega = 0$ for operation at the design wavelength λ_0.[10] To comply with the condition that $d\Phi/d\omega = 0$, mirrors with anomalous dispersion (AD) to provide the desired reflectance phase are required. An AD mirror can be made by use of a PC with one or more defects. High reflectance is achieved when the Bragg condition is satisfied, i.e., when $n_H d_H + n_L d_L = \lambda_0/2$, where n_H (n_L) and d_H (d_L) are the high (low) refractive index and the corresponding thickness of the material layers, respectively.

Consider a 1-D PC made from seven layers, LHLHLHL [Fig. 1(b), inset], where H and L, respectively, represent the quarter-wave thicknesses of GaAs and Al_xO_y layers with corresponding refractive indices $n_H = 3.374$ and $n_L = 1.50$ for a design wavelength of 1550 nm (i.e., $H = \lambda_0/4$, $L = \lambda_0/4$, and the corresponding physical thickness of the H or the L layer is $\lambda_0/4n_H$ and $\lambda_0/4n_L$). One can convert a given layer into a defect by increasing the thickness of that layer, thereby altering the reflectance and the reflectance phase of the stack. Figure 1(b) shows the reflectance phase of a PC with different locations of the defect. The desired AD reflectance phase is obtained when the defect is located in the fifth or sixth layer. In addition, as the location of the defect is moved from the fifth to the sixth layer, the region of anomalous reflectance phase increases but the slope at 1550 nm decreases with wavelength. The slope of the AD phase needs to be chosen to compensate for the phase variation of $\omega c^{-1} nd\cos\theta$ acquired by off-resonance frequency waves propagating in the cavity. Use of these AD mirrors in designing the bandpass filter generates a flat-topped transmission band. Figure 1(c) shows the transmittance of a flat-topped bandpass filter designed with two identical AD mirrors, each of which has a defect in its sixth layer, and a resonator cavity of $\lambda_0/2$ optical thickness. To compensate for the phase shift caused by the cavity and produce unity transmittance at λ_0, the optimized optical thickness of the defect in the AD mirror has to be $2.5\lambda_0$.

B. Wide-Angle Field of View

Next we consider the dependence of the filter's transmittance properties on the angle of the incident radiation. It is well known that as the incidence angle increases, not only does the center of the resonant transmission band shift to shorter wavelengths but its shape is also altered. For example, consider an AD mirror composed of layers $L_1H_1L_1H_1L_1H_2L_1$, where L_1 and H_1 represent the optical thicknesses of the GaAs and Al_xO_y layers, respectively, and satisfy the relation $L_1 + H_1 = \lambda_0/2$. H_2 is the optical thickness of the defect in the AD mirror that causes the resonance to occur at 1550 nm. The 15-layer bandpass filter can be described by $H|L_1H_2L_1H_1L_1H_1L_1H_3L_1H_1L_1H_1L_1H_2L_1|H$, where H_3 is the optical thickness of resonant cavity C and determines the transmittance spectrum. Here we define a parameter: optical thickness ratio $\eta = H_1/L_1$. Figure 2(a) depicts examples of the transmittance of this structure with $\eta = 0.67, 1.00, 2.33, 4.00$ for incidence angles of 0°, 25°, and 50°, respectively, in air. As the incidence angle increases, we find not only that the transmittance at 1550 nm decreases to val-

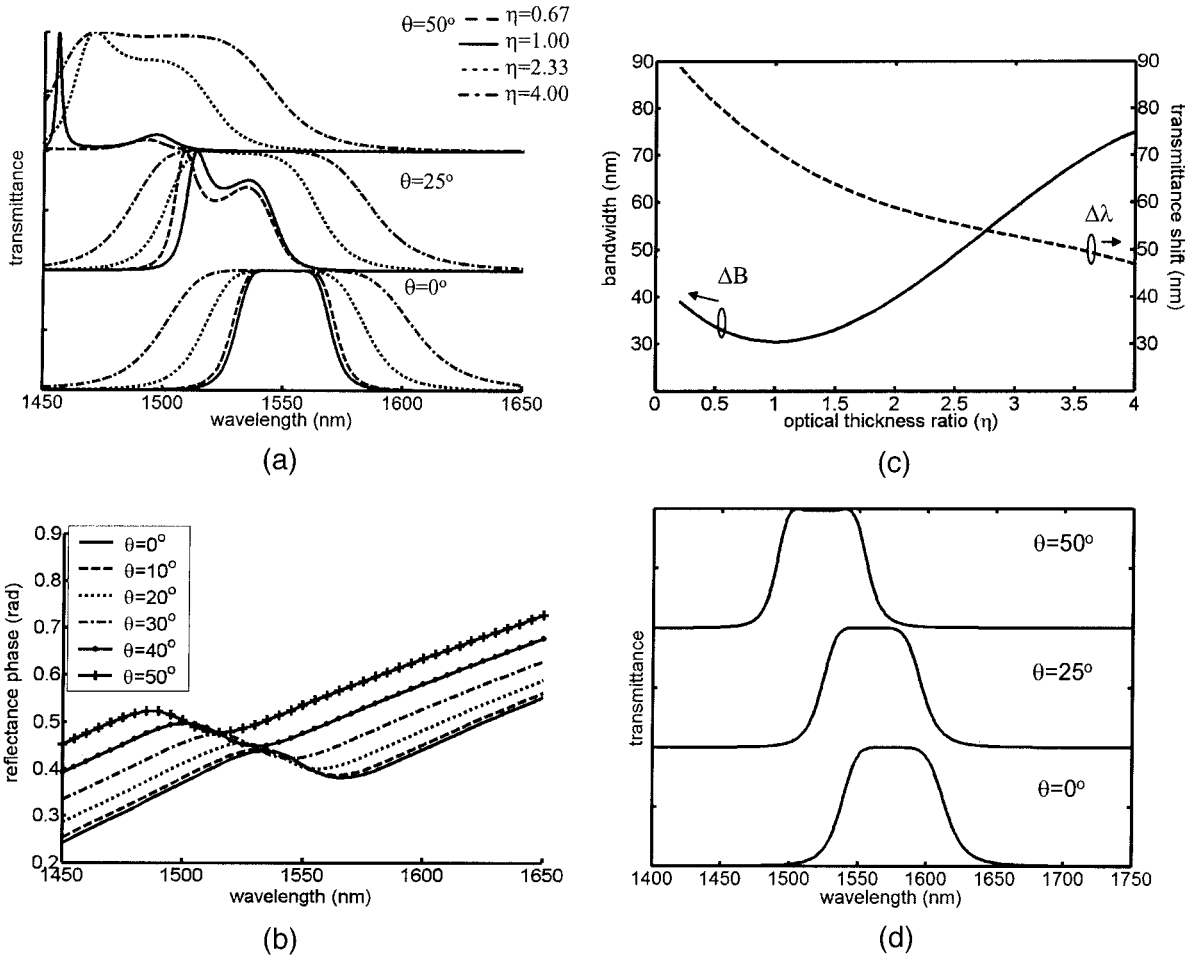

Fig. 2. (a) Bandpass filter designs with four optical thickness ratios η analyzed for transmittance with three incidence angles θ. The filter is $H|L_1H_2L_1H_1L_1H_1L_1H_3L_1H_1L_1H_1L_1H_2L_1|H$ with optical thickness ratio $\eta = H_1/L_1$. For $\eta = 0.67$, $b = 9.84$, and $c = 1.87$. For $\eta = 1$, $H_2 = 10H$ and $H_3 = 2H$. For $\eta = 2.33$, $H_2 = 6.29H$ and $H_3 = 2.26H$. For $\eta = 4$, $H_2 = 6.46H$ and $H_3 = 2.42H$. The results were calculated for TE polarization. (b) Reflectance phases of the AD mirror with $\eta = 2.33$ and six incidence angles θ. (c) Shift of the center wavelength of filter $\Delta\lambda_{50}$ and filter bandwidth ΔB of a 15-layer flat-topped bandpass filter versus η. We found spectrum shift $\Delta\lambda_{50}$ by changing the incidence angle from 0 to 50°, and bandwidth ΔB is the range where the transmittance is larger than 0.9 at normal incidence. (d) Transmittance of the designed filter at three incidence angles θ.

ues less than 1 but also that the shape of the transmittance curve is distorted for small values of η. In addition, as η increases, the bandwidth increases and the spectrum shift decreases. Figure 2(a) indicates that parameter η can be used to optimize the desired field of view. In the optimization process we would like to determine the cavity material and the optical thickness ratio η of the AD mirrors by considering the following characteristics of the filter: spectrum shift, deviation from normal of the transmittance at the design wavelength, and filter bandwidth.

In the design process we begin with the material of the cavity. The actual optical path inside the medium decreases as the incidence angle increases (i.e., the optical thickness of the cavity in a Fabry–Perot structure is $nd \cos\theta$, and, as the incidence angle increases, the center of the transmittance spectrum shifts to a shorter wavelength). It is evident from Snell's law that to minimize the effect of the angle of incidence we should use a high-refractive-index material (e.g., GaAs) in the cavity to minimize the shift of the center wavelength of the transmittance band of the filter. For example, for a half-wave thickness layer and an incidence angle in air that varies from 0 to 50°, the corresponding wavelength shift caused by a defect in the GaAs layer will be only 40 nm.

The second parameter that we use in our design is the optical thickness ratio (η) of the AD mirrors. To reduce angular selectivity we use a GaAs substrate material with the seven-layer AD mirror structure $L_1H_1L_1H_1L_1H_2L_1$. First we consider obtaining high transmittance independently of the angle of incidence at the design wavelength (1550 nm). This implies that for center wavelength λ_0 we would like to achieve invariance in θ for a total phase shift Φ [Eq. (2)] with the approximate value $(2m + 1)\pi$ such that Eq. (1) is invariant in θ. This condition can be satisfied when the variation of the phase change caused by the cavity length is equal to the variation of the phase on reflection from the AD mirrors. It is evident from

Eq. (2) that, as the incidence angle increases, the phase variation that is due to the cavity length decreases. Next we examine the variation of the phase on reflection from the AD mirrors as the incidence angle increases. Fortunately, the reflectance phase of the AD mirrors in the AD region at the design wavelength also decreases as the angle of incidence increases, compensating for the phase variation of Φ.[11] It was shown in Ref. 11 that the reflectance phase is related to the wavelength and to the total optical thickness of the multilayer structure. However, as the incidence angle is tilted, the total optical thickness is also reduced. Consequently the reflectance phase in the AD region is reduced, approximately in proportion to the total optical thickness. Figure 2(b) shows an example of the reflectance phase of the AD mirror, $H|L_1H_1L_1H_1L_1H_2L_1|H$ with $\eta = 2.33$, with several incidence angles. The reflectance phase in the AD region is reduced as the incident wave is tilted, whereas outside this regime it is increased. In this instance, however, at incidence angles larger than 20° the reflectance phase at 1550 nm increases with incidence angle. The anomalous region of the reflectance phase and the reflectance spectrum of the AD mirrors shift to shorter wavelengths simultaneously with the incidence angle. Additionally, the width of the AD region determines the bandwidth of the bandpass filter.[10] Therefore the bandwidth of the bandpass filter has to be designed to be larger than the amount of spectral shift of the AD mirrors within the desired range of the variation of the incidence angles to produce high transmittance at λ_0.

First, we define two parameters: $\Delta\lambda_\theta$, the shift of the center wavelength of the bandpass filter as the incidence angle is changed from 0° to θ°, and filter transmission bandwidth ΔB, which is defined by the wavelength range for transmittance larger than 0.9 at normal incidence. Figure 2(c) shows $\Delta\lambda_{50}$ and ΔB variations of a 15-layer flat-topped bandpass filter structure, $H|L_1H_2L_1H_1L_1H_1L_1H_3L_1H_1L_1H_1L_1H_2L_1|H$, for various values of optical thickness ratio η. We can observe that $\Delta B(\eta)$ is a minimum at $\eta = 1$, whereas $\Delta\lambda_{50}(\eta)$ is a monotonically decreasing function. The two curves intersect at an optical thickness ratio of approximately $\eta = 2.8$, showing that, for an optical thickness ratio larger than 2.8, the amount of the spectrum shift is smaller than the bandwidth of the bandpass filter and can be ignored, making a good approximation to our desired filter performance design.

Using the thickness ratio $\eta = 2.8$ obtained in the discussion above yields a thickness of the GaAs layer (H_1) of 160.5 nm and of the Al_xO_y layer (L_1) of 131.3 nm. Because there are different media on the two sides of the cavity, a modification of the seventh layer is necessary to produce approximately unity transmittance at 1550 nm at normal incidence. The structure of the AD mirror next to air is changed to $L_1H_1L_1H_1L_1H_{2'}L_{1'}H_{1'}|$air; and that next to the substrate, to $L_1H_1L_1H_1L_1H_{2''}L_{1''}|H$. Hence the total number of layers in the final design is 16. $L_{1'}$, $H_{1'}$, and $L_{1''}$ are adjusted to produce the same reflectance of the structures $H|L_{1'}H_{1'}|$air and $H|L_{1''}|H$ at 1550 nm. In addition, $H_{2'}$ and $H_{2''}$ have to be adjusted to yield the resonance of two AD mirrors at 1550 nm.

From Fig. 2(b) we know that ΔB is roughly 54 nm at the intersection point. Consequently the choices of $L_{1'}$, $H_{1'}$, $L_{1''}$, $H_{2'}$, and $H_{2''}$ have to achieve a bandwidth of the AD region larger than 54 nm. The thicknesses of $L_{1'}$, $H_{1'}$, and $L_{1''}$ are 92.9, 214.3, and 195.3 nm, respectively. The thickness of $H_{2'}$ is 493.5 nm, whereas that of $H_{2''}$ is 502.7 nm. Then, by positioning these two AD mirrors in opposition, we adjust H_3 to achieve a flat-topped passband, in this case 515.4 nm. The transmittance of the final design for TE-polarization incidence with incidence angles of $\theta = 0°, 25°, 50°$ is shown in Fig. 2(d). The FWHM at normal incidence is 76.4 nm and at ΔB is 53 nm. In addition, the wavelength shift is 51.67 nm as the incidence angle is changed from 0° to 50°, which is smaller than ΔB, as desired.

3. Fabrication of the Filter

We used the filter design procedure discussed in Section 2 to construct a filter made from a multilayer structure of the high-refractive-index contrast materials GaAs/Al_xO_y. The fabrication approach was based on growing a multilayer structure of GaAs/AlAs, followed by oxidation to convert AlAs into Al_xO_y. Special samples were designed, fabricated, and characterized to determine the index of refraction of the oxidized Al_xO_y. This procedure is essential because, in the literature,[12–16] the value of the refractive index of the oxidized AlAs may vary in the range 1.49–1.65, depending on the initial material, oxidation procedures, and conditions. We then used these specific experimentally determined parameters to design and fabricate the filter as described below.

Binary GaAs/AlAs multilayers were grown by MBE at 600 °C. Nominal film thicknesses were calibrated *in situ* by reflection high-energy electron diffraction measurements, but actual values were determined by *ex situ* optical normal incidence reflection and angularly dependent transmission measurements that are described below. Grown layer structures were then patterned with trenches of 10 μm on 110-μm centers. The mesa structures were defined by a nonselective sulfuric acid wet etch, and these etched samples were then immediately oxidized.

There has been extensive investigation of lateral wet oxidation of AlAs and AlGaAs layers.[12] It is well established that the oxidation of binary AlAs leads to instability in the layers, which then tend to delaminate from the substrate. There are at least three mechanisms that may play roles in this delamination process: the strain induced by the linear contraction on a change of the AlGaAs/AlAs layers into the native oxide (Al_xO_y); the oxidation of GaAs, which is known to have a brittle, unstable oxide, in the normal direction, and the various remaining volatile As-containing waste products that do not completely diffuse out of the layers after the oxidation reac-

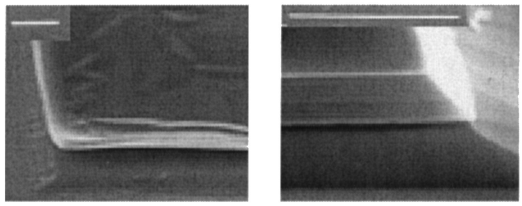

Fig. 3. (a) Scanning-electron microscope image of the fabricated mesa structure and subsequent delamination. (b) Mesa structure intact after *in situ* annealing as described in the text. Scale for bars in both images, 10 μm.

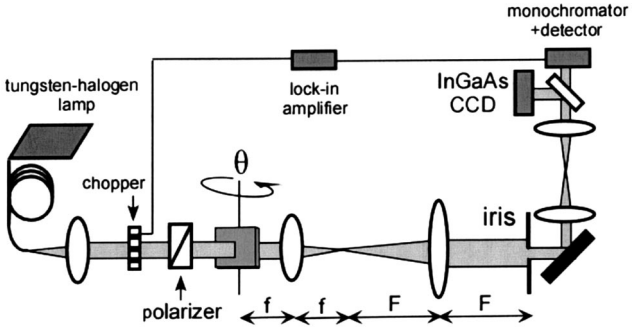

Fig. 4. Apparatus for optical characterization. The broadband incident beam is collimated and polarized. The sample is then 4*f* imaged via a lens onto a pinhole for alignment and control of the measurement area and 4*f* imaged again onto an InGaAs CCD and spectrum analysis setup.

tion.[12,17] It remains unclear which of these mechanisms is the most important in causing mechanical instabilities.

In our fabrication process the oxidation proceeds in a 1-in.- (2.54-cm-) diameter tube furnace, which is maintained at 420 ± 2 °C. Nitrogen is bubbled through water maintained at ~85 °C at a nominal rate of 500 mL/min. Rates are calibrated with a separate sample, and we terminate the reaction by switching to a dry-nitrogen flow soon after complete oxidation of the layers. The nitrogen flow rate is simultaneously reduced to less than 100 mL/min. The temperature of the furnace is reduced to 400 °C for the required anneal time. Filter structures with and without *in situ* annealing are shown in Figs. 3(a) and 3(b), respectively. Although significant improvement is observed in stability—with a considerable portion remaining fully intact and thus measurable—these devices have not shown a 100% yield, with a small number delaminating as shown in Fig. 3(a). We are continuing to try to remedy this problem by changing the alloy's composition and optimizing the anneal process as far as possible; it must be noted that thicker layers can be oxidized more readily with sufficient stability when a small amount of Ga remains in the AlGaAs alloy. This procedure comes, however, at the expense of a decreased oxidation rate, ultimately affecting the potential size of the device.

4. Apparatus for Characterization and Procedures

To measure the transmission of relatively small devices in a large range of angles of incidence we have adopted a configuration analogous to confocal imaging, as shown in Fig. 4. A variable-aperture pinhole is imaged from the transmitted side onto the device to be measured. Illumination from a broadband tungsten halogen source is limited to a spot size of ~50-μm diameter on the device to be measured. In this way, a low-power microscope objective with a long working distance is utilized without inhibiting rotation of the sample to large incidence angles. Samples are lapped and polished, and an InGaAs CCD array is used for imaging and alignment. The signal is simultaneously sent to a scanning monochromator–photodetector apparatus to measure the spectral response from 1000 to ~1700 nm (limited in this case by the response of the InGaAs photodiode).

A. Measurement of Oxidized AlAs Index of Refraction

To obtain satisfactory results in the performance of the filter it has been deemed necessary to characterize the index of refraction for the oxidized AlAs layers from our specific growth and oxidation processes. Because of the delamination problem, there are few data for thickly oxidized AlAs layers beyond ~1 μm.[14–16] To determine the index of refraction we adopted a method similar to that of Heremans *et al.*[18] in that the angular dependence of the resonance shift of an oxidized Fabry–Perot structure is examined, with the difference that we make the measurement in the transmission mode instead of on reflection.

The Fabry–Perot structure consists of two periods of nominally quarter-wave GaAs/Al_xO_y bottom Bragg mirror layers, followed by a half-wavelength Al_xO_y cavity layer and finished with a 2.5-period GaAs/Al_xO_y top Bragg mirror. The fabricated mesas are then measured at multiple angles of incidence with two polarizations, and we make a fit to the resonant wavelength by varying only the linear contraction and the index of refraction for the oxidized Al_xO_y layers [see Fig. 5(a)]. The dispersion properties of the GaAs layers are determined from the literature.[19]

Results of this fit are shown in Fig. 5(b), with good agreement for TE and TM polarization. The value of the oxide index from our process was determined to be $n = 1.50$, and the linear contraction of the AlAs was 13.5%. Oxidized AlAs were studied, and large variations in the refractive index of this material were reported.[14–18] Results seem to be process dependent from lab to lab are to be particularly sensitive to the starting material and even, in one study, to be sensitive to both time and carrier-gas composition and purity.[16] Our value is in agreement with those of a subset of authors when it is considered that we are working with both significantly thicker layers and a longer wavelength than for other measurements starting from binary AlAs versus ternary AlGaAs layers.

We also used this cavity structure to calibrate the

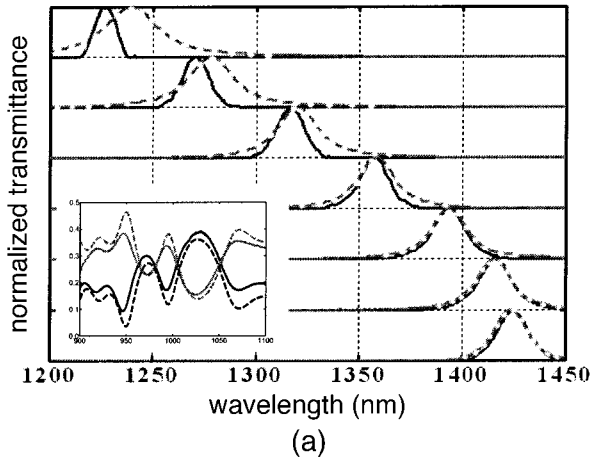

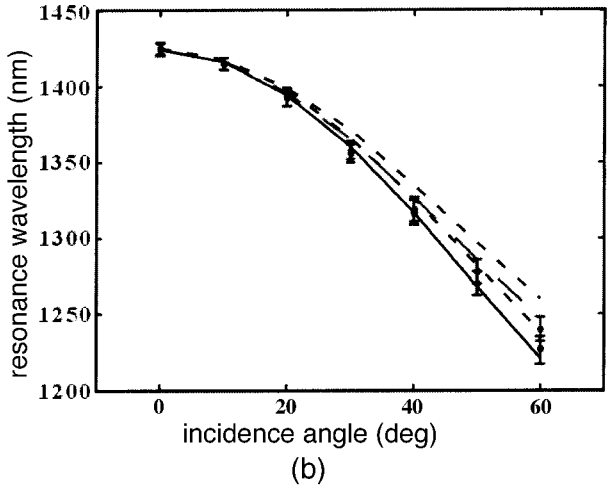

Fig. 5. (a) Measured transmittance data utilized to determine the index of refraction and amount of layer shrinkage of the oxide. Solid (dashed) curves, to TE (TM) polarization. Inset, normal-incidence transmittance (reflectance) data illustrated by solid darker (lighter) curves. We fitted the predicted values (dashed curves) to determine the thickness of the initial epitaxial layer. (b) Simultaneous fitting of the index of refraction and shrinkage of the oxide layers. The resonance of the Fabry–Perot structure is then fitted at various angles of incidence for both TE and TM polarization (solid curves) to yield the two quantities of interest. For comparison, a similar fit is shown with an oxide index value of 1.55 (dashed curves); the resonance values did not fit at higher incidence angles.

layer growth rates, and thus the structure had significantly less than the intended thickness. In what follows, we assume that the dispersion of the oxide index is negligible over this range of wavelengths, which is a reasonable approximation[16] for this wavelength range.

B. Optimized Filter Design and Characterization

We used these calibration results in filter design and optimization by including layer growth rates, AlAs oxide shrinkage, and measured index of refraction. The structure consists of a GaAs buffer layer followed by the layers listed in Table 1. Actual thicknesses

Table 1. Designed Thicknesses of the 15-Layer Filter

Layer	Composition of Layer	Design Thickness (nm)	
		As Grown	Oxidized
1	AlAs	224.5	195.3
2	GaAs	502.7	502.7
3	AlAs	150.9	131.3
4	GaAs	160.5	160.5
5	AlAs	150.9	131.3
6	GaAs	160.5	160.5
7	AlAs	150.9	131.3
8	GaAs	515.4	515.4
9	AlAs	150.9	131.3
10	GaAs	160.5	160.5
11	AlAs	150.9	131.3
12	GaAs	160.5	160.5
13	AlAs	150.9	131.3
14	GaAs	493.5	493.5
15	AlAs	106.8	92.9
16	GaAs	214.3	214.3

were again determined optically—in this case with an error of ~1.5%—which resulted in a shift in the center wavelength of the passband of ~23 nm.

Measured transmission spectra for TE polarization at normal incidence are shown in Fig. 6(a). In this curve the dispersion of GaAs was included for an accurate fit of the spectral features of the transmission beyond the stop band of the filter below ~1300 nm, whereas the oxide was considered dispersion free with constant index 1.50 as determined above. The measured values were found to be in good agreement with the calculations over the whole spectral range from 1000 to 1700 nm. All results are shown normalized to the transmission maximum that is due to Fresnel reflection from the back surface of the substrate, which changes with the angle of incidence, with a maximum of more than 90%. Figure 6(b) shows details of the behavior of the transmission band as a function of angle of incidence for the TE polarization, offset by angle of incidence for clarity. The wavelength shift over the angle change from 0° to 50° was 44 nm, which is quite close to the expected design value of 51.67 nm. Additionally, $\Delta B = 37.4$ nm at normal incidence. As noted above, the transmittance band tends to narrow for the TE polarization as expected—from ~65 nm FWHM at normal incidence to 57 nm at 50°, which are slightly smaller than the predicted values of 76.4 and 67 nm, respectively.

5. Summary and Discussion

In summary, we have demonstrated the design, fabrication, and characterization of a resonant spectral filter with a wide stop band and a flat-topped passband based on a GaAs/Al_xO_y material system. The design method provides an analytic and systematic approach to simultaneously optimizing the pass bandwidth, shape, and angular sensitivity characteristics. We optimized the design of the multiple-defect

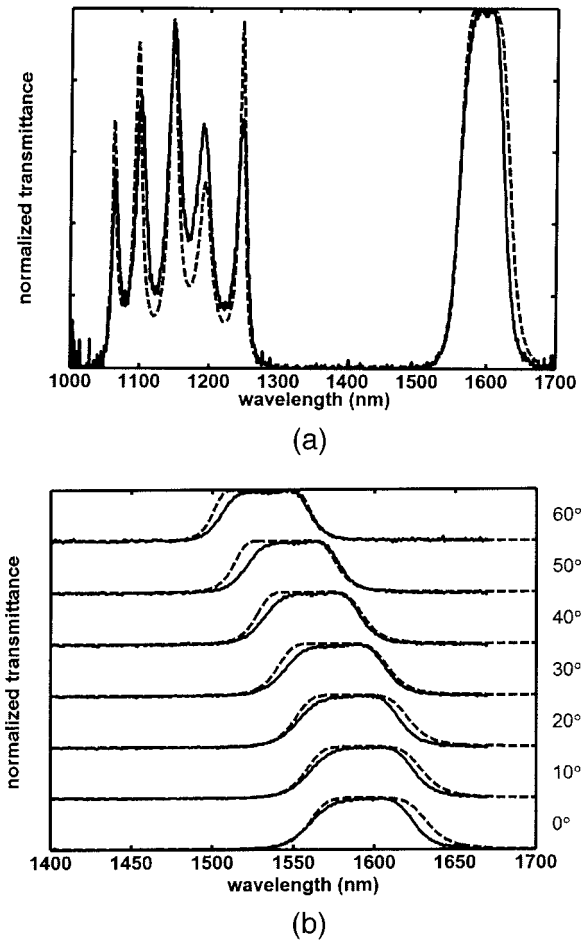

Fig. 6. (a) Normal-incidence transmittance of the filter, showing the stop band and the narrow transmission band. Measured data are shown by the solid curve; the calculated values, with an oxide index of 1.50, are shown dashed. Dispersion in the GaAs is accounted for to accurately fit the data in the lower wavelength regime. (b) Transmittance for various angles of incidence. The solid and dashed curves correspond to the measured data and to the data calculated by transfer matrix methods, respectively.

1D PC-based filter by adjusting the optical thickness ratio of the anomalous-dispersion Bragg mirror layers in a high-index-contrast materials system. In addition, the optimized design incorporates the experimentally determined optical properties of the oxidized GaAs/Al_xO_y layers to facilitate good agreement between the calculated and measured results.

A flat-topped bandpass filter design for center wavelength 1550 nm with a FWHM of 76.4 nm and a wavelength shift of 51.67 nm as the incidence angle is varied from 0 to +50° has been presented. Experimental characterization of the fabricated device showed a center wavelength at 1600 nm with a FWHM of 65 nm and a wavelength shift of 44 nm as the incidence angle varied from 0 to +50°. The experimental results are in good agreement with the design when the spectrum's shift to longer wavelength that results from a roughly 1.5% thickness error in the fabrication of each layer is taken into consideration.

This structure has the advantage of a single epitaxial growth step that is compatible with current detector growth technology, followed by a single chemical etching step and a well-established oxidation step. As noted, a filter of this type would be useful for incorporation into an integrated detector for a free-space optical communications system. We shall seek to incorporate a detector element in the filter structure. For use at 1550 nm, a similar structure could be grown amorphously upon an epitaxially grown InP-based detector structure[20]; alternatively, a similar design approach could be used to incorporate an InGaAsN detector[21] at 1300 nm in the central cavity, providing resonant enhancement to increase quantum efficiency.

The support of the Defense Advanced Research Projects Agency, the U.S. Air Force Office of Scientific Research, the National Science Foundation, and Applied Micro Circuits Corporation/California's Communications Research (CORE) program is gratefully acknowledged.

References

1. A. Thelen, *Design of Optical Interference Coatings* (McGraw-Hill, New York, 1989), p. 20.
2. H. A. Macleod, *Thin-Film Optical Filters*, 3rd ed. (Institute of Physics, Philadelphia, Pa., 2001).
3. M. F. Weber, C. A. Stover, L. R. Gilbert, T. J. Nevitt, and A. J. Ouderkirk, "Giant birefringent optics in multilayer polymer mirrors," Science **287,** 2451–2455 (2000).
4. J. R. Barry, *Wireless Infrared Communications* (Kluwer Academic, Boston, Mass., 1994), pp. 17–35.
5. Y. Fu and N. K. A. Bryan, "Design of hybrid micro-diffractive-refractive optical element with wide field of view for free space optical interconnections," Opt. Express **10,** 540–548 (2002), http://www.opticsexpress.org.
6. S. Jivkova and M. Kavehrad, "Holographic optical receiver front end for wireless infrared indoor communications," Appl. Opt. **40,** 2828–35 (2001).
7. W. Nakagawa, P.-C. Sun, C.-H. Chen, and Y. Fainman, "Wide-field-of-view narrow-band spectral filters based on photonic crystal nanocavities," Opt. Lett. **27,** 191–193 (2002).
8. Y. Fink, J. N. Winn, S. Fan, C. Chen, J. Michel, J. D. Joannopoulos, and E. L. Thomas, "A dielectric omnidirectional reflector," Science **282,** 1679–1682 (1998).
9. Y. Park, Y.-G. Roh, C.-O. Cho, and H. Jeona, "GaAs-based near-infrared omnidirectional reflector," Appl. Phys. Lett. **82,** 2770–2772 (2003).
10. Y. V. Troitski, "Dispersion-free, multiple-beam interferometer," Appl. Opt. **34,** 4717–4722 (1995).
11. A. V. Tikhonravov, P. W. Baumeister, and K. V. Popov, "Phase properties of multilayers," Appl. Opt. **36,** 4382–4392 (1997).
12. See, for example, K. D. Choquette, K. M. Geib, C. I. H. Ashby, R. D. Twesten, O. Blum, H. Q. Hou, D. M. Follstaedt, B. E. Hammons, D. Mathes, and R. Hull, "Advances in selective wet oxidation of AlGaAs alloys," IEEE J. Sel. Top. Quantum Electron. **3,** 916–926 (1997), and references therein.
13. H. Q. Jia, H. Chen, W. C. Wang, W. X. Wang, W. Li, Q. Huang, J. Zhou, and Q. K. Xue, "Improved thermal stability of wet oxidized AlAs," Appl. Phys. Lett. **80,** 974–976 (2002).
14. K. J. Knoop, R. P. Mirin, D. H. Christensen, K. A. Bertness, A. Roshko, and R. A. Synowicki, "Optical constants of $(Al_{0.98}Ga_{0.02})_xO_y$ native oxides," Appl. Phys. Lett. **73,** 3512–3514 (1998).
15. P. Sifkis, P. Paddon, V. Pcradouni, M. Adamcyk, C. Nicoll, A.

R. Cowan, T. Tiedje, and J. F. Young, "Near-infrared refractive index of thick, laterally oxidized AlGaAs cladding layers," J. Lightwave Technol. **18,** 199–202 (2000).
16. D. C. Hall, H. Wu, L. Kou, Y. Lou, R. J. Epstein, O. Blum, and H. Hou, "Refractive index and hydroscopic stability of $Al_xGa_{1-x}As$ native oxides," Appl. Phy. Lett. **75,** 1110–1112 (1999).
17. S.-K. Cheong, B. A. Bunker, T. Shibata, D. C. Hall, C. B. DeMelo, Y. Luo, G. L. Snider, G Kramer and N. El-Zein, "Residual arsenic site in oxidized $Al_xGa_{1-x}As$ (x - 0.96)," Appl. Phys. Lett. **78,** 2458–2460 (2001).
18. P. Heremans, M. Kuijk, R. Windisch, J. Vanderhaegen, H. De Neve, R. Vounckx, and G. Borghs, "Angular spectroscopic analysis: an optical characterization technique for laterally oxidized AlGaAs layers," J. Appl. Phys. **82,** 5265–5267 (1997).
19. E. Palik, *Handbook of Optical Constants of Solids* (Academic, New York, 1985).
20. D. E. Wohlert, H. C. Lin, K. L. Chang, G. W. Pickrell, Jr., J. H. Epple, K. C. Hsieh, and K. Y. Chen, "Fabrication of a substrate-independent aluminum oxide-GaAs distributed Bragg reflector," Appl. Phys. Lett. **75,** 1371–1373 (1999).
21. Z. Pan, L.-H. Li, Y.-Q. Xu, W. Zhang, Y.-W. Lin, R.-K. Zhang, Y. Zhong, and X.-M. Ren, "GaInNAs/GaAs multiple-quantum well resonant-cavity-enhanced photodetectors at 1.3 μm," Chin. Phys. Lett. **18,** 1249–1251 (2001).